Biomass burning related ozone damage on vegetation over the Amazon forest: A model sensitivity study.

F. Pacifico[1], G. A. Folberth[2], S. Sitch[3], J. M. Haywood[1,2], L. V. Rizzo[5], F. F. Malavelle, and P. Artaxo[4]

[1] College of Engineering, Mathematics and Physical Sciences, University of Exeter, Exeter, UK
[2] Met Office Hadley Centre, Exeter, UK
[3] Geography, College of Life and Environmental Sciences, University of Exeter, Exeter, UK
[4] Department of Applied Physics, Institute of Physics, University of Sao Paulo, Sao Paulo, Brazil
[5] Department of Earth and Exact Sciences, Institute of Environmental, Chemical and Pharmaceutics Sciences, Federal University of Sao Paulo, Sao Paulo, Brazil

Abstract

The HadGEM2 Earth System climate model was used to assess the impact of biomass burning on surface ozone concentrations over the Amazon forest and its impact on vegetation, under present-day climate conditions. Here we consider biomass burning emissions from wildfires, deforestation fires, agricultural forest burning, residential and commercial combustion. Simulated surface ozone concentration is evaluated against observations taken at two sites in the Brazilian Amazon forest for years 2010 to 2012. The model is able to reproduce the observed diurnal cycle of surface ozone mixing ratio at the two sites, but overestimates the magnitude of the monthly averaged hourly measurements by 5-15 ppb for each available month at one of the sites. We vary biomass burning emissions over South America by +/-20, 40, 60, 80 and 100% to quantify the modelled impact of biomass burning on surface ozone concentrations and ozone damage on vegetation productivity over the Amazon forest. We used the ozone damage scheme in the "high" sensitivity mode to give an upper limit for this effect. Decreasing South American biomass burning emissions by 100% (i.e. to zero) reduces surface ozone concentrations (by about 15ppb during the biomass burning season) and suggests a 15% increase in monthly mean net primary productivity averaged over the Amazon forest, with local increases up to 60%: this gives us an estimate of the effect of current biomass burning on plant productivity. The simulated impact of ozone damage from present-day biomass

35 burning on vegetation productivity is about 230 TgC/yr. Taking into account that uncertainty in
36 these estimates is substantial, this ozone damage impact over the Amazon forest is of the same
37 order of magnitude as the release of carbon dioxide due to fire in South America; in effect to
38 potentially double the impact of biomass burning on the carbon cycle.
39

Introduction

Biomass burning is a global source of aerosol and trace gases, including ozone (O_3) precursors, and can lead to local and regional O_3 pollution. Tropospheric O_3 is a greenhouse gas and, above background concentrations, an air pollutant: it is harmful to human health (e.g. Lippmann 1993; Burnett et al., 1997) and it damages plants (e.g. Rich et al., 1964; Fiscus et al., 2005; Felzer et al., 2007; Ainsworth et al., 2012). Tropospheric O_3 is a product of photochemical reactions whose main precursors are nitrogen oxides (NO_x), carbon monoxide (CO), methane (CH_4) and volatile organic compounds (VOCs) (Seinfeld and Pandis, 1998). VOCs are particularly important in Amazonia because of the large natural biogenic and biomass burning emissions (Karl et al., 2007).

In the Amazon forest, biomass burning is mostly anthropogenic, and mainly occurs during the dry season (August to October). Biomass burning emissions drastically change the composition of the atmosphere, e.g. diurnal maximum mixing ratios of tropospheric O_3 varies from 12 parts per billion (ppb), during the wet season, to values as high as 100 ppb in the biomass burning affected dry season (Kirkman et al., 2002, Sigler et al., 2002, Artaxo et al., 2002, 2005, Rummel et al., 2007).

Surface O_3 mixing ratios over 40 ppb are known to produce visible leaf injury and damage to plants, reducing crop productivity and posing a threat to food security; nonetheless different climatic conditions (e.g. soil moisture and water stress) also play a role in determining leaf stomatal closure and hence there will be variable impacts of the same O_3 concentrations (Ashmore, 2005), e.g. tropical rainforest vegetation may be particularly sensitive to surface O_3, even at concentrations below 40ppb (a threshold associated with extra-tropical vegetation), due to high stomatal conductances. Moreover, tropical vegetation evolved in low background O_3 concentrations and could be more sensitive to O_3. In leaves, cellular damage caused by O_3 not only reduces photosynthetic rates but also requires increased resource allocation to detoxify and repair leaves (Ainsworth et al., 2012). Ozone damage to vegetation reduces plant productivity, decreasing the amount of carbon absorbed by plants, hence has an impact on climate via and indirect radiative forcing (Sitch et al., 2007).

Tropical rain forests play an important role in the global carbon budget, as they cover 12% of the Earth's land surface and contain around 40% of the terrestrial biosphere's carbon (Ometto et al., 2005, Taylor & Lloyd, 1992). It has been estimated that they may account for as much as 50% of the global net primary productivity (Grace et al., 2001). Depending on age, land use and large scale

meteorological conditions, tropical forest ecosystems can act as net carbon sources, sinks, or they can be in approximate balance (Lloyd. et al., 2007, Gatti et al., 2013), but it is uncertain if global environmental changes are forcing these ecosystems outside their range of natural variation (Sierra et al., 2007). However, biomass burning may further reduce natural sinks in the neighbouring intact forest, via air pollution and O_3 damage on vegetation, and thus current estimates of the effects of biomass burning on the carbon cycle (Le Quéré et al., 2009) may be underestimated. Biomass burning is also an important aerosol source: regional levels of particulate matter are very high in the dry season in Amazonia (Artaxo et al., 2013), and the increase in diffuse radiation due to changes in aerosol loadings can increase net ecosystem exchange (NEE) quite significantly (Oliveira et al., 2007, Cirino et al., 2013). After a certain level of aerosol optical depth, the decrease in radiation fluxes can reduce significantly NEE over Amazonia (Cirino et al., 2013). This study does not consider the effects of the changes in diffuse radiation due to biomass burning on photosynthesis, or the impact of aerosols on O_3 chemistry via changing photolysis rate. That will be the focus of a separate study. Our specific aim is to estimate the effect of O_3-induced changes on vegetation productivity due to biomass burning.

Importantly, Sitch et al. (2007) performed their assessment of the potential impact of O_3 on vegetation using an offline simulation where monthly mean O_3 concentrations derived with a global chemistry climate model were used in determining the impacts of O_3 damage. Here we use an online flux-gradient approach to quantify the impact of biomass burning on surface O_3 concentration and O_3 damage on vegetation over the Amazon forest (see model description). The HadGEM2 (Hadley Centre Global Environment Model 2; Collins et al., 2011; Martin et al., 2011) Earth System climate model is used to study these interactions. We show results of the evaluation of surface O_3 simulated with HadGEM2 against observations in the Amazon forest and model experiments quantifying the impact of biomass burning on plant productivity.

Methods

We used HadGEM2 to simulate surface O_3 concentrations and O_3 damage on vegetation for present-day (2001-2009) climate conditions. Our version of HadGEM2 includes the O_3 damage scheme developed by Sitch et al. (2007). We evaluated simulated surface O_3 against observations taken at two sites in the Amazon forest: Porto Velho (Brazil; 8.69°S; 63.87°W), a site heavily impacted by biomass burning emissions, and site ZF2 in the Cuieiras forest reserve in Central Amazonia (Brazil;

2.59°S; 60.21°W). A description of the sites can be found in Artaxo et al. (2013). In a sensitivity study we varied biomass burning emissions over South America by +/-20, 40, 60, 80, 100% to quantify the potential impact of biomass burning on surface O_3 concentrations and O_3 damage over the Amazon forest.

Model description

HadGEM2 is a fully coupled Earth-system model (Collins et al., 2011). It is built around the HadGEM2 atmosphere-ocean general circulation model and includes a number of earth system components: the ocean biosphere model diat-HadOCC (Diatom-Hadley Centre Ocean Carbon Cycle, a development of the HadOCC model of Palmer and Totterdell, 2001), the Top-down Representation of Interactive Foliage and Flora Including Dynamics (TRIFFID) dynamic global vegetation model (Cox, 2001), the land-surface and carbon cycle model MOSES2 (Met Office Surface Exchange Scheme; Cox et al. 1998, 1999; Essery et al. 2003), the interactive Biogenic Volatile Organic Compounds (iBVOC) emission model (Pacifico et al., 2012), the United Kingdom Chemistry and Aerosol (UKCA) model (O'Connor et al., 2014) and an interactive scheme of O_3 damage on vegetation (Sitch et al., 2007; Clark et al., 2011).

The configuration used here is a version of HadGEM2-UKCA with extended tropospheric chemistry (N96L38), the resolution is 1.25° latitude x 1.875° longitude (~200 x 140 km) with 38 vertical levels extending up to 39 km altitude. The land-based anthropogenic, biomass burning, and shipping emissions are taken from Lamarque et al. (2010), and represent a decadal (1997-2006) mean centered on the year 2000. The use of an emission pattern from 1997-2006 can lead to an overestimation of O_3 concentrations by the model, since the emissions vary on a year to year basis and are expected to be lower in recent years due to the reduction in Amazonian deforestation via burning, consequently reducing the amount of O_3 precursors. HadGEM2 runs at a 30 minute time step with the exception of global radiation, which is updated every 3 hours and provides radiative fluxes between those time steps via interpolation. This configuration is described and evaluated in O'Connor et al. (2014) with the exception of the Extended Tropospheric Chemistry (ExtTC) that has been applied in this work. The ExtTC mechanism has been designed to represent the key species and reactions in the troposphere in as much detail as is necessary to simulate atmospheric composition-climate couplings and feedbacks while retaining the capability to conduct decade-long climate simulations. UKCA-ExtTC simulates the spatial distribution and evolution in time of 89

141 chemical species, 63 of which are model tracers. The model includes emissions from anthropogenic,
142 biogenic, soil, and wildfire sources for 17 species: nitrogen oxides (NO_x = NO +NO_2), CH_4, carbon
143 monoxide (CO), hydrogen (H_2), methanol, formaldehyde, acetaldehyde and higher aldehydes,
144 acetone, methyl ethyl ketone, ethane (C_2H_6), propane (C_3H_8), butanes and higher alkanes, ethene
145 (C_2H_4), propene (C_3H_6), isoprene, (mono)terpenes, and a lumped species representing aromatics
146 (toluene + xylene) from anthropogenic sources.
147
148 Emissions of biogenic species (isoprene, terpenes, methanol, acetone) are computed by iBVOC and
149 provided to UKCA at every time step. The isoprene emission scheme is that of Pacifico et al.
150 (2011). Terpenes, methanol, and acetone emissions are simulated with the model described in
151 Guenther et al. (1995). Anthropogenic and wildfire emissions are prescribed from monthly mean
152 emission data sets prepared for CMIP5 using the historic scenario (Lamarque et al., 2010). Given
153 the difficulty in prescribing a diurnal cycle for fire emissions, these monthly mean emissions are
154 kept constant during the day. Wetland methane emissions are prescribed from data from Gedney et
155 al. (2004). Soil-biogenic NO_x emissions are prescribed using the monthly distributions provided by
156 the Global Emissions Inventory Activity (http://www.geiacenter.org/inventories/present.html),
157 which are based on the global empirical model of soil-biogenic NO_x emissions of Yienger and Levy
158 (1995). NO_x emissions from global lightning activity are parameterized based on the convective
159 cloud top height following Price and Rind (1992, 1994) and are thus sensitive to the model climate.
160 UKCA also includes a dry deposition scheme based on the resistance in-series approach as outlined
161 in Wesely (1989). Physical removal of soluble species is parameterized as a first-order loss process
162 based on convective and stratiform rainfall rates (Collins et al., 2011).
163
164 The TRIFFID vegetation module of HadGEM2 simulates the dynamics of five plant functional
165 types (PFTs): broadleaf trees, needleleaf trees, shrubs, and C_3 and C_4 grass (i.e., grasses using the
166 C_3 and C_4 photosynthetic pathway, respectively). Changes in the extent of croplands over time are
167 not simulated but are prescribed from land use maps prepared for the Coupled Model
168 Intercomparison Project 5 (CMIP5, Taylor et al., 2012). Here we use the historic (1850–2000; Hurtt
169 et al., 2009) data sets, as described in Jones et al. (2011). A further four surface types (urban, inland
170 water, bare soil, and ice) are used in the land-surface scheme for the calculation of water and energy
171 exchanges between the land and the atmosphere. Each model grid box can include varying
172 proportions of several vegetation and/or surface types. The model does not include interactive
173 deforestation due to fire.
174

The parameterization of O_3 damage on vegetation is that of Sitch et al., (2007). This scheme uses a flux-gradient approach to model O_3 damage, rather than empirical approaches based on the accumulated O_3 exposure above 40 ppb (e.g. Felzer, et al. 2005). The Sitch et al. (2007) parameterization assumes a suppression of net leaf photosynthesis by O_3 that varies proportionally to the O_3 flux through stomata above a specified critical O_3 deposition flux. The critical deposition flux depends on O_3 concentration near the leaves, but also on stomatal conductance. This scheme also includes a relationship between stomatal conductance and photosynthesis, determining a reduction in stomatal conductance through O_3 deposition. As the O_3 flux itself depends on the stomatal conductance, which in turn depends upon the net rate of photosynthesis, the model requires a consistent solution for the net photosynthesis, stomatal conductance and the O_3 deposition flux. This approach to modelling O_3 effects on photosynthesis accounts for the complex interaction between CO_2 and O_3 effects, and can be used to study future climate impacts. This scheme includes a 'high' and 'low' parameterization for each PFT to represent species more sensitive and less sensitive to O_3 effects; in our analysis we use the 'high' sensitivity mode to establish the maximum response. The model was calibrated with data from temperate and boreal vegetation. Calibration data for other ecosystems, including tropical vegetation, are currently unavailable.

Description of the model experiments

All simulations use HadGEM2 in its atmosphere-only configuration, i.e., with all implemented couplings between atmosphere and land surface (including carbon cycle) active but without the atmosphere-ocean coupling. HadGEM2 was initialized with equilibrium concentrations of the major chemical components (O_3, CO, H_2, total reactive nitrogen (NO_y), BVOCs) taken from the CMIP5 simulation (see description of the simulations in Jones et al., 2011). Methane mixing ratios were prescribed as specified by CMIP5, with values of 1750 ppb for present-day. The decade-mean CO_2 atmospheric mixing ratio was 368 ppm.

Monthly means of sea surface temperature and sea ice cover were prescribed using climatologies derived from the appropriate decade of the Hadley Centre CMIP5 transient climate run Jones et al., (2011). The vegetation distribution for each of our simulations was prescribed using the simulated vegetation averaged for the same decade from this transient climate run, on which we superimposed crop area as given in the CMIP5 historic and future land use maps (Hurtt et al., 2009; Riahi et al., 2007).

We performed a 9-year (2001-2009) control simulation for present-day climate conditions

209 initialized from a centennial transient climate simulation with ocean couplings (Jones et al., 2011).
210 We analysed the last 8 years of the simulation, as the first year of simulation was used as spin-up. A
211 single year is considered sufficient for spin-up because one year is around five times longer than the
212 lifetime of the longest lived atmospheric species (with the exclusion of methane) involved in O_3
213 chemistry. The control simulation was driven by anthropogenic and wildfire emissions of trace
214 gases and aerosols via historical scenarios (Global Fire Emissions Database GFEDv2; Lamarque et
215 al., 2010; Van der Werf et al., 2006) of anthropogenic and wildfire emissions. We also perform 10
216 experiments that differ from the control simulation in terms of assumed biomass burning emissions,
217 i.e. biomass burning emissions over South America are either increased or decreased by +/-20, 40,
218 60, 80, 100%, while emissions over the rest of the world are kept unchanged. The vegetation
219 distribution was not adjusted for loss of vegetation due to fire. We define biomass burning
220 emissions as those from wildfires, deforestation fires, agricultural forest burning, residential and
221 commercial combustion, including fuel wood burning, charcoal production and biofuel combustion
222 for cooking and heating (Lamarque et al., 2010). The dominant fire types in South America are
223 from deforestation and degradation fires in an arc around Amazonia, with some regional hotspots of
224 agricultural burning (see Figure 13 in Van der Werf et al., 2010). Between 2001 and 2009 the
225 percentage contribution to annual fire emissions from fire types (deforestation and degradation,
226 grassland and savanna, woodland, forest, agriculture) are (59%, 22%, 10%, 8%, 2%) over Southern
227 Hemisphere South America (Figure 13 van der Werf et al., 2010), with minor differences in this
228 region between this dataset (Global Fire Emissions Database GFEFv3) and the earlier GFEDv2 used
229 in this study (see Fig. 16 in Van der Werf et al., 2010).
230
231 This set of experiments allows us to simulate the impact of biomass burning on surface O_3 and
232 vegetation productivity. The control simulation was also used to evaluate surface O_3 mixing ratios
233 against measurements over the Amazon forest.
234
235
236 **Model site-level Evaluation**
237
238 Over the data-sparse Amazonian region, comprehensive spatial data sets of surface O_3
239 concentration are extremely limited. We evaluated simulated surface O_3 against observations from
240 two sites that have full annual analyses of O_3 concentration: Porto Velho (Brazil; 8.69°S; 63.87°W)
241 and site ZF2 in the Cuieiras forest reserve (Brazil; 2.59°S; 60.21°W). O_3 mixing ratios were

measured with a UV absorption analyser (Thermo 49i, USA). Observations from both sites have an estimated 4% uncertainty, considering zero noise, zero and span drifts reported in the instrument manual, and the frequency of zero and span checks performed along the experiments.

The Porto Velho sampling site is located in a forest reserve about 5 km NE (generally upwind) from the city of Porto Velho. Large land use change and regional biomass burning makes its atmospheric conditions characteristic of those of the Amazon forest with significant human interference (Brito et al., 2014). The whole region of Porto Velho has been subject to land use change since the 1980s. In Porto Velho, the dry season is from June to October and the wet season from November to May. Measurements of surface O_3 mixing ratios were taken from November 2011 to October 2012 in a forest clearance, at 5 m a.g.l..

The Cuieiras forest reserve in Central Amazonia encloses 380 km^2 of pristine tropical rainforest forest. The reserve is located in the central Amazon Basin, 60 km NNW of downtown Manaus and 40 km from the metropolis margins. This site is relatively undisturbed, as no biomass burning occurs in the forest reserve. Here rain showers are frequent with a short dry season from July to October. Measurements were taken at 39 m a.g.l. at the TT34 tower. The forest canopy height near the tower varied between 30 and 35 m, and the site is described in Martin et al. (2010), Rizzo et al. (2013) and Artaxo et al. (2013). Most of the time, the prevailing trade winds blow over 2000 km of the intact tropical forest before reaching the measurement tower. However, the site was also affected by regional transport of pollutants, either from biomass burning or urban (Rizzo et al., 2013). Measurements of surface O_3 mixing ratios were taken from April 2010 to June 2012, with the exclusion of a few months due to instrument maintenance.

We compared simulated (averaged over 8 years of simulations) against observed average diurnal cycle at each site for each available month. The model overestimates observed monthly averaged hourly O_3 mixing ratios at the surface by about 5-15 ppb for all months at the Porto Velho site, but it reproduces the diurnal and seasonal cycle, including those months affected by biomass burning, i.e. August and September, at the Porto Velho site (Figure 1). The model is able to reproduce the diurnal cycle, including magnitude, at the ZF2 site for about 8 months out of 24. The model overestimates surface monthly averaged hourly O_3 mixing ratios by about 5-10 ppb for the rest of months, which are also the months with lower surface O_3 mixing ratios (Figure 2).

276 **Results**

277

278 Our analysis is focused on the region enclosed in the red rectangle in figure 3, this is a highly
279 vegetated region with homogeneous topography, and it includes the two sites used for the model
280 evaluation (Porto Velho and ZF2 in the Cuieiras forest reserve). This region of analysis is covered
281 by two PFTs in HadGEM2: broadleaf trees, which is the predominant, and C_3 grass (Figure 3).

282

283 Surface O_3 mixing ratios simulated with HadGEM2 are higher during the months of August,
284 September and October over the Amazon forest, and in particular over our region of analysis,
285 because of the higher biomass burning emissions in the model during these months. Monthly
286 average surface O_3 mixing ratios in our control simulation peaks at 55-60 ppb in this region (Figure
287 4), while the average over the region of analysis is peaked at about 30 ppb in August and
288 September, less in October (Figure 5a, black line).

289

290 Monthly total Net Primary Productivity (NPP) in our control simulation reaches its minimum
291 during the months of August and September (Figure 5b, black line), at about 300 TgC/month,
292 corresponding to the end of the dry season.

293

294 Decreasing biomass burning emissions over South America by -20%, -40%, -60%, -80%, -100%
295 decreases surface O_3 mixing ratios and increases net productivity. Vice versa, increasing biomass
296 burning emissions over South America by +20%, +40%, +60%, +80%, +100% increases surface O_3
297 mixing ratios over the region of analysis and subsequently reduces net productivity because of O_3
298 damage on vegetation (Figure 5c).
299 These sensitivity tests suggest that decreasing biomass burning emission by 100% over South
300 America brings monthly mean surface O_3 mixing ratios averaged over the region of analysis to
301 about the observed 15 ppb for each month (Figure 5a, dark blue line), even during the dry season,
302 with no values over 35 ppb for any grid-cell (Figure 6). Increasing biomass burning emissions by
303 100% suggests that monthly mean mixing ratios of surface O_3 averaged over the region of analysis
304 reach 40 ppb in August (Figure 5a), with peaks of about 65-70 ppb in some grid-cells (Figure 6a).
305 For both increases and decreases of between 20 and 80% in South American biomass burning the
306 model simulates almost linear changes in surface O_3 mixing ratios (Figure 6, the figure shows
307 increases and reductions by 40, 60 and 100%).

308

Suppressing biomass burning emissions (i.e. decreasing biomass burning emission by 100%) over South America increases total NPP over the region of analysis by about 15%, to about 350-370 TgC/month, with peak increases of 60% for a few grid-cells, in August and September (Figure 6b): this quantifies the impact of present-day biomass burning on vegetation productivity. When increasing biomass burning emissions over South America by 100%, monthly total NPP over the region of analysis is reduced by about 10%, i.e. to about 250 TgC/month, in August and September (Figure 5b), with peak values of 50-60% reductions for few grid-cells (Figure 6c). For reductions by 20 to 80% in South American biomass burning the model varies NPP almost linearly (Figure 5c). However, the increase in South American biomass burning by 20 to 80% determine a very similar decrease in NPP, e.g. between 7 and 10% decrease in August (Figure 5c). Both increasing and reducing South American biomass burning from 20 to 80% increases the number of grid-cells where a significant variation of NPP takes place (Figure 6b). The percentages given above are significant against inter-annual variability in the control simulation, i.e. we only take into account of the variations above one standard deviation in the control simulation. We also exclude from our analysis the grid-cells with low productivity, i.e. where NPP in the control simulation is below 50 gC/m^2/month (i.e. we focus on high productivity regions, e.g. forests).

Discussion and Conclusions

The HadGEM2 model overestimates the magnitude of the O_3 diurnal cycle at the two sites used in the evaluation. Overestimation of simulated O_3 in the Amazonian boundary layer has been observed in other modelling studies, especially in clean air conditions (Bela et al., 2014). Nonetheless, our model reproduces the main features of the diurnal and seasonal cycle. In particular, the model is able to reproduce the increase in surface O_3 during the biomass burning season.

As stated earlier in the model description section, biomass burning emissions are prescribed as monthly mean and kept constant during the day, and this can have an impact on the hourly and day-to-day variation of surface O_3. For example, O_3 production will respond differently if biomass burning emissions occur during the day or at night, affecting simulated surface O_3 mixing ratios. These issues can be improved by modelling fire and biomass burning emissions interactively. The inclusion of an interactive fire model in HadGEM is currently under development.

342 The model overestimates surface O_3 mixing ratios by 5-15 ppb for several months at the ZF2 site in
343 the Cuieiras forest reserve and for all available months at the Porto Velho site. The reasons for these
344 systematic biases in surface O_3 mixing ratio are likely manifold. In a complex, highly coupled
345 system such as the HadGEM2 Earth System Model (ESM) it is not always easy to disentangle all
346 processes and attribute model biases to specific components.
347 We attribute the systematic biases in the surface O_3 mixing ratio to the following, most likely
348 reasons:
349 1. Model resolution in both the horizontal and the vertical dimension
350 2. Uncertainties in emissions, both magnitude, seasonality and location
351 3. Uncertainties in the O_3 dry deposition at the surface
352 Other factors such as photolysis rates, lightning NO_x production over the area and transport of O_3
353 and precursors will certainly contribute. We will briefly discuss the three most important (in our
354 opinion) factors that contribute to the systematic biases.
355
356 The relatively coarse resolution of a global ESM simulates mixing ratios of trace species (both trace
357 gases and aerosols) that represent averages over large areas. This issue has been discussed
358 previously in the literature, mostly in relation to air quality modelling (see, e.g., Valari and Menut,
359 2008; Tie et al., 2010; Appel et al. 2011; Thompson and Selin, 2012). In our case one grid box
360 equals approximately 30,000 km^2 (i.e., 200x150 km^2 in longitude and latitude). The implicit
361 averaging pertains both to emission and concentration fields; the predominant consequence is a
362 dilution in each grid-cell. Depending on the chemical regime, this can lead to reduced or enhanced
363 net O_3 production. Additionally, HadGEM2-ES has a relatively coarse vertical resolution.
364 HadGEM2-ES has a lowest model layer depth of 48m (global average) and the vertical profile of O_3
365 will undoubtedly show a gradient as the loss mechanism for O_3 is dominated by the surface (e.g.
366 Colbeck and Harrison, 1967). The measurement level may explain part of the model overestimation,
367 since it is well known that O_3 mixing ratios strongly decrease with height due to deposition within
368 the canopy. The lowest layer of the model is 48 m (which corresponds to canopy top over vegetated
369 grid-cells), while measurements were taken at 5 m and 39 m a.g.l. respectively at Porto Velho and
370 ZF2. Rummel et al. (2007) reports a 5-15 ppb O_3 decrease from 52 to 11 m a.g.l. in a forest site in
371 Amazonia.
372
373 The remote environment of the Amazon forest is dominated by relatively high concentrations of
374 VOC, particularly of biogenic origin, and low concentrations of nitrogen oxides, NO_x. It is a NO_x-
375 limited environment. In such an environment O_3 is destroyed by reactions with BVOC (mainly

376 isoprene and (mono-)terpenes). This destruction is more pronounced the higher the BVOC
377 concentration becomes. Consequently, conditions in the global model are likely to differ from that
378 of a measurement at a specific point such as those we compare to in Figures 1 and 2. It is a known
379 problem in model evaluation.
380
381 Another issue related to model resolution, when comparing global models to point-like
382 observations, is the uncertainty in global emission inventories, both with respect to magnitude and
383 location. In particular the latter will result in discrepancies between modelled concentrations of O_3
384 and its precursors and point-like observations. But the uncertainties in emission magnitude are also
385 substantial and can reach a factor of two or more in case of biogenic VOC (e.g., Guenther et al.,
386 2006; Arneth et al., 2008, 2011; Pacifico et al., 2011, 2012).
387
388 Thirdly, and again related to model resolution, is the representation of O_3 dry deposition at the
389 surface. Its magnitude and diurnal cycle will depend on boundary layer turbulence, surface
390 roughness, land surface type, vegetation type, soil moisture, photosynthetic activity, and more. In a
391 recent sensitivity study by Folberth et. al (in preparation) O_3 surface concentrations showed the
392 largest sensitivity to perturbations in O_3 surface dry deposition fluxes. Underestimating O_3 surface
393 dry deposition, in particular during the night preventing a complete flush of the PBL with respect to
394 O_3, will lead to systematic biases.
395
396 Interestingly, however, the latter process may also represent a redeeming feature of the model.
397 According to our model of O_3 plant damage it is the total O_3 flux into the plant that determines the
398 amount of damage caused to the photosynthetic activity and, hence, carbon assimilation. However,
399 the total O_3 flux (or dose) is a function of both O_3 surface concentrations and dry deposition, i.e. for
400 plants there is a compensation effect when concentrations are overestimated while deposition
401 velocities are underestimated. Underestimating the O_3 dry deposition flux implies reduced O_3 plant
402 uptake, and consequently an underestimation of the plant damage and productivity losses. However,
403 it also leads to higher O_3 concentrations, which subsequently act to increase plant O_3 uptake and
404 damage, compensating for the initial effects on productivity. Still, a detailed assessment and
405 quantification of this interdependence of O_3 concentration and dry deposition fluxes is beyond the
406 scope of this study and must be referred to future research.
407
408 August, September and October are the months when biomass burning and surface O_3
409 concentrations are higher over the Amazon forest, but also the months when plant productivity is at

its lowest which will tend to suppress the impact of O_3 damage on plant productivity. This is because stomatal conductance is reduced due to water limitations (also accounted for in the model) during the dry season, thus reducing the flux of both carbon dioxide and O_3 into the leaves, and consequently reducing O_3 plant damage.

Ashmore (2005), noted how O_3 exposure is poorly correlated with flux into leaves and also the potential for damagingly high O_3 fluxes in leaves at concentrations significantly below 40 ppb at maximum stomatal conductance. Consequently, global vegetation models as used in this study have adopted flux-based parameterizations to represent O_3 impacts on vegetation, moving away from application of the earlier exposure based metrics, e.g. accumulated O_3 exposure above a threshold of 40 ppb, AOT40.

The parameterization of O_3 damage used in this study is calibrated for high-latitude vegetation. Unfortunately data for calibrating this O_3 damage scheme for tropical vegetation are currently not available and observations of O_3 damage in the Amazon forest are very limited. Observations of O_3 damage on tropical forests are urgently needed, including observations at moderate (e.g. 20-30 ppb) and high surface O_3 mixing ratios.

The simulated impact of present-day biomass burning on vegetation productivity over our area of analysis is about 230 TgC/yr (i.e. the difference between the dark blue line and the black line in Fig. 5b) using the "high" sensitivity mode in the O_3 damage scheme. Taking into account that the uncertainty in these estimates is substantial, this O_3 damage impact over the Amazon forest is of the same order of magnitude as the release of CO_2 due to land fire in South America, as quantified in van der Werf et al., (2010; 293 TgC/yr from table 7 of that paper); in effect to potentially double the impact of biomass burning on the CO_2 fluxes. This highlights the urgent need for more tropical data on plant O_3 damage to better constrain estimates.

Despite overestimating surface O_3 mixing ratios our model simulates only a moderate reduction in NPP associated with elevated O_3 due to biomass burning emissions. Given that our model systematically overestimates O_3 mixing ratio, assuming accurate dry deposition, and that we use our model in the high sensitivity mode, our simulations where we increase biomass burning emissions by 100% suggest a maximum 10% average reduction in monthly plant productivity, and peak reductions of 50-60% reductions in few grid-cells. This is because, despite the increase in biomass burning, monthly average surface O_3 mixing ratios do not exceed a moderate 40 ppb. Moreover, our

model does not include deforestation due to fire, which would reduce vegetation cover when increasing biomass burning emissions in our sensitivity experiments, reducing NPP, and BVOC emissions, further. However, local and daily/hourly impact of O_3 damage on plant productivity can be higher.

Estimates of the magnitude of the reduction in plant productivity due to O_3 damage can be improved with additional field studies and improving the representation of tropospheric O_3 in ESMs (sources, chemistry and sinks). Nevertheless, considering these processes in a coupled system can provide an improvement in robustness of conclusions, as e.g. it can treat processes with a specific diurnal cycle, like photosynthesis and surface O_3, interactively on a short time scale (e.g. half an hour in our model).

Acknowledgments

This work was funded by the Natural Environment Research Council (NERC) South AMerican Biomass Burning Analysis (SAMBBA) project grant code NE/J010057/1. The UK Met Office contribution to this project was funded by the DECC under the Hadley Centre Climate Programme contract (GA01101). The Brazilian contribution was funded by Fundacao de Amparo a Pesquisa do Estado de Sao Paulo (FAPESP, projects 08/58100-2 and 12/14437-9). We thank INPA (Instituto Nacional de Pesquisas da Amazonia) for the coordination work of the LBA Experiment. We thank USP technicians for the support on data sampling: Alcides Ribeiro, Ana Lucia Loureiro, Fernando Morais and Fabio Jorge.

References

Ainsworth, E. A., Yendrek, C. R., Sitch, S., Collins, W. J. and Emberson, L. D.: The Effects of Tropospheric Ozone on Net Primary Productivity and Implications for Climate Change, Annu. Rev. Plant Biol., 63, 637-61, 2012.

Appel, K. W., Foley, K. M., Bash, J. O., Pinder, R. W., Dennis, R. L., Allen, D. J. and Pickering, K.: A multi-resolution assessment of the Community Multiscale Air Quality (CMAQ) model v4.7 wet deposition estimates for 2002-2006, Geosci. Model Dev., 4, 357-371, 2011.

Arneth, A., Monson, R. K., Schuregers, G., Niinemets, Ü. and Palmer, P. I.: Why are estimates of global terrestrial isoprene emissions so similar (and why is it not so for monoterpenes), Atmos. Chem. Phys., 8, 4605-4620, 2008.

Arneth, A., Schurgers, G., Lathiere, J., Duhl, T., Beerling, D. J., Hewitt, N., Guenther, A.: Global terrestrial isoprene emission in models: sensitivity to variability in climate and vegetation, Atmos. Chem. Phys., 11, 8037-8052, 2011.

Artaxo, P., Martins, J. V., Yamasoe, M. A., Procópio, A. S., Pauliquevis, T. M., Andreae, M. O., Guyon, P., Gatti, L. V., Leal., A. M. C.: Physical and chemical properties of aerosols in the wet and dry season in Rondônia, Amazonia. J. Geophys. Res., 107, D20, 8081-8095, 2002.

Artaxo, P., Gatti, L V., Leal, A. M. C, Longo, K. M., de Freitas, S. R., Lara, L. L., Pauliquevis, T. M., Procópio, A. S., Rizzo, L. V.: Atmospheric Chemistry in Amazonia: The forest and the biomass burning emissions controlling the composition of the Amazonian atmosphere, Acta Amazonica, 35(2), 185-196, 2005.

Artaxo, P., Rizzo, L. V., Brito, J. F., Barbosa, H. M. J., Arana, A., Sena, E. T., Cirino, G. G., Bastos, W., Martin, S. T., Andreae. M. O.: Atmospheric aerosols in Amazonia and land use change: from natural biogenic to biomass burning conditions. Faraday Discussions, 2013

Ashmore, M. R: Assessing the future global impacts of ozone on vegetation, Plant Cell Environ., 28, 949-964, 2005.

Bela, M. M., Longo, K. M., Freitas, S. R., Moreira, D. S., Beck, V., Wofsy, S. C., Gerbig, C., Wiedemann, K., Andreae, M. O., and Artaxo, P.: Ozone production and transport over the Amazon Basin during the dry-to-wet and wet-to-dry transition seasons, Atmos. Chem. Phys. Discuss., 14, 14005–14070, 2014

Brito, J., Rizzo, L. V., Morgan, W. T., Coe, H., Johnson, B., Haywood, J., Longo, K., Freitas, S., Andreae, M. O. and Artaxo, P.: Ground based aerosol characterization during the South American Biomass Burning Analysis (SAMBBA) field experiment, Atmos. Chem. Phys. Discuss., 14, 12279-12322, 2014.

Burnett, R. T., Brook, J. R., Yung, W. T., Dales, R. E., Krewski, D.: Association between Ozone and Hospitalization for Respiratory Diseases in 16 Canadian Cities, Environ. Res., 72, 1, 24-31, 1997.

Cirino, G.G., Souza, R. F., Adams, D. K. and Artaxo, P.: The effect of atmospheric aerosol particles and clouds on net ecosystem exchange in Amazonia, Atmos. Chem. Phys. Discuss., 13, 28819–28868, 2013.

Clark, D. B., Mercado, L. M., Sitch, S., Jones, C. D., Gedney, N., Best, M. J., Pryor, M., Rooney, G. G., Essery, R. L. H., Blyth, E., Boucher, O., Harding, R. J., Huntingford, C. and Cox, P. M.: The Joint UK Land Environment Simulator (JULES), model description – Part 2: Carbon fluxes and vegetation dynamics, Geosci. Model Dev., 4, 701-722, 2011.

Colbeck, I. and Harrison, R. M.: Dry deposition of ozone: some measurements of deposition velocity and of vertical profiles to 100 metres, Atm. Environ., 19, 11, 1807-1818, 1967

Collins, W. J., Bellouin, N., Doutriaux-Boucher, M., Gedney, N., Halloran, P., Hinton, T., Hughes, J., Jones, C. D., Joshi, M., Liddicoat, S., Martin, G., O'Connor, F., Rae, J., Senior, C., Sitch, S., Totterdell, I., Wiltshire, A. and Woodward, S.: Development and evaluation of an Earth-system model-HadGEM2, Geosci. Model Dev., 4, 1051–1075, 2011.

Cox, P. M., Huntingford, C. and Harding, R. J.: A canopy conductance and photosynthesis model for use in a GCM land surface scheme, J. Hydrol., 212–213, 79–94, 1998.

533 Cox, P. M., Betts, R. A., Bunton, C. B., Essery, R. L. H., Rowntree, P. R. and Smith, J.: The impact
534 of new land surface physics on the GCM simulation of climate and climate sensitivity, Clim. Dyn.,
535 15, 183–203, 1999.
536
537 Cox, P. M.: Description of the "TRIFFID" Dynamic Global Vegetation Model, Tech. Note 24, 17
538 pp., Met Off. Hadley Cent., Exeter, U. K, 2001.
539
540 Essery, R. L. H., Best, M. J., Betts, R. A., Cox, P. M. and Taylor, C. M.: Explicit representation of
541 subgrid heterogeneity in a GCM Land Surface Scheme, J. Hydrometeorol., 4, 530–543, 2003.
542
543 Felzer, B., Reilly, J., Melillo, J., Kicklighter, D., Sarofim, M., Wang, C., Prinn, R. and Zhuang, Q.:
544 Future effects of ozone on carbon sequestration and climate change policy using a global
545 biogeochemical model, Clim. Change 73, 345–373, 2005.
546
547 Felzer, B. S., Cronin, T., Reilly, J. M., Melillo, J. M. and Wang, X.: Impacts of ozone on trees and
548 crops, C. R. Geosci., 339, 784–798, 2007.
549
550 Fiscus, E. L., Booker, F. L., Burkey, K. O.: Crop responses to ozone: uptake, modes of action,
551 carbon assimilation and partitioning, Plant Cell Environ, 28, 997-1011, 2005.
552
553 Folberth, G. A., Abraham, N. L., Dalvi, M., Johnson, C. E., Morgenstern, O., O'Connor, F. M.,
554 Pacifico, F., Young, P. A., Collins, W. J., and Pyle, J. A.: Evaluation of the new UKCA climate-
555 composition model. Part IV. Extension to Tropospheric Chemistry and Biogeochemical Coupling
556 between Atmosphere and Biosphere, Geosci. Model Dev. (in preparation)
557
558 Gatti et al.: Drought sensitivity of Amazonian carbon balance revealed by atmospheric
559 measurements, Nature 506, 76-80, 2014.
560
561 Gedney, N., Cox, P. M. and Huntingford, C.: Climate feedback from wetland methane emissions,
562 Geophys. Res. Lett., 31, L20503, 2004.
563
564 Grace, J., Mahli, Y., Higuchi, N., Meir, P.,: Productivity and carbon fluxes of tropical rain forest.
565 In: J.Roy, H.A.M. (Ed). Global Terrestrial Productivity. Academic Press, San Diego, 2001.
566

567 Guenther, A., Hewitt, C. N., Erickson, D., Fall, R., Geron, C., Graedel, T., Harley, P., Klinger, L.,
568 Lerdau, M., Mckay, W. A., Pierce, T., Scholes, B., Steinbrecher, R., Tallamraju, R., Taylor, J., and
569 Zimmerman, P.: A global model of natural volatile organic compound emissions, J. Geophys. Res.,
570 100(D5), 8873– 8892, 1995.
571
572 Guenther, A., Karl, T., Harley, P., Wiedinmyer, C., Palmer, P. I. and Geron, C.: Estimates of global
573 terrestrial isoprene emissions using MEGAN (Model of Emissions of Gases and Aerosols from
574 Nature), Atmos. Chem. Phys., 6, 3181-321-, 2006.
575
576 Hurtt, G. C., et al.: Harmonization of global land-use scenarios for the period 1500–2100 for IPCC-
577 AR5, iLEAPS Newsl., 7, 6–8, 2009.
578
579 Jones, C. D., et al.: The HadGEM2-ES implementation of CMIP5 centennial simulations, Geosci.
580 Model Dev. Discuss., 4(1), 689–763, 2011.
581
582 Karl, T., Yokelson, R., Guenther, A., Greenberg, J., Blake, D., Artaxo, P.: TROFFEE (TROpical
583 Forest and Fire Emissions Experiment): Investigating Emission, Chemistry, and Transport of
584 Biogenic Volatile Organic Compounds in the Lower Atmosphere over Amazonia. J. Geophys. Res.,
585 112, (D18), D18302, 2007.
586
587 Kirkman, G. A., Gut, A., Ammann, C., Gatti, L. V, Cordova, A. M., Moura, M. A. L., Meixner, F.
588 X.: Surface exchange of nitric oxide, nitrogen dioxide, and ozone at a cattle pasture in Rondônia,
589 Brazil, J. Geophys. Res., 107(D20), 8083, 2002.
590
591 Kvalevag M. M., Myhre, G.: The effect of carbon-nitrogen coupling on the reduced land carbon
592 sink caused by tropospheric ozone, Geophys. Res. Letters, 40, 1-5, 2013.
593
594 Lamarque, J.-F., et al.: Historical (1850–2000) gridded anthropogenic and biomass burning
595 emissions of reactive gases and aerosols: Methodology and application, Atmos. Chem. Phys., 10,
596 7017–7039, 2010.
597
598 Le Quéré, C. M. R., Raupach, J. G., Canadell, G. Marland et al.: Trends in the sources and sinks of
599 carbon dioxide, Nature Geosciences, 2, 2009.
600

601 Lippmann, M.: Health effects of tropospheric ozone: review of recent research findings and their
602 implications to ambient air quality standards, J. Exp. An. Environ. Epid., 3(1), 103-129, 1993.
603
604 Lloyd. J., Kolle, O., Fritsch, H., de Freitas, S. R., Dias, M. A. F. Silva, Artaxo, P., Nobre, A. D., de
605 Araujo, A. C., Kruijt, B., Sogacheva, L., Fisch, G., Thielmann, A., Kuhn, U., Andreae, M. O.: An
606 airborne regional carbon balance for Central Amazonia, Biogeosciences 4 (5): 759-768, 2007.
607
608 Martin, S. T., Andreae, M. O., Althausen, D., Artaxo, P., Baars, H., Borrmann, S., Chen, Q.,
609 Farmer, D. K., Guenther, A., Gunthe, S. S., Jimenez, J. L., Karl, T., Longo, K., Manzi, A., Müller,
610 T., Pauliquevis, T., Petters, M. D., Prenni, A. J., Pöschl, U., Rizzo, L. V., Schneider, J., Smith, J. N.,
611 Swietlicki, E., Tota, J., Wang, J., Wiedensohler, A., and Zorn, S. R.: An overview of the
612 Amazonian Aerosol Characterization Experiment 2008 (AMAZE- 08), Atmos. Chem. Phys., 10,
613 11415-11438, 2010.
614
615 Martin, G. M., et al.: The HadGEM2 family of Met Office Unified Model Climate configurations,
616 Geosci. Model Dev., 4, 723–757, 2011.
617
618 O'Connor, F. M., Johnson, C. E., Morgenstern, O., Abraham, N. L., Braesicke, P., Dalvi, M.,
619 Folberth, G. A., Sanderson, M. G., Telford, A. Voulgarakis, P. J., Young, P. J., Zeng, G., Collins,
620 W. J. and Pyle, J. A.: Evaluation of the new UKCA climate-composition model – Part 2: The
621 Troposphere, Geosci. Model Dev., 7, 41-91, 2014.
622
623 Oliveira, P. H. F., Artaxo, P., Pires Jr, C., de Lucca, S., Procópio, A., Holben, B., Schafer, J.,
624 Cardoso, L. F., Wofsy, S. C., Rocha, H. R.: The effects of biomass burning aerosols and clouds on
625 the CO_2 flux in Amazonia, Tellus Series B-Chemical and Physical Meteorology, 59B, (3) 338–349,
626 2007.
627
628 Ometto, J. P., Nobre, A. D., Rocha, H., Artaxo, P., Martinelli, L.: Amazônia and the Modern
629 Carbon Cycle: Lessons Learned. Oecologia, 143, 4, 483-500, 2005.
630
631 Pacifico, F., et al.: Evaluation of a photosynthesis-based biogenic isoprene emission scheme in
632 JULES and simulation of isoprene emissions under present-day climate conditions, Atmos. Chem.
633 Phys., 11, 4371–4389, 2011.
634

635 Pacifico, F., Folberth, G. A., Jones, C. D., Harrison, S. P. and Collins, W. J.: Sensitivity of biogenic
636 isoprene emissions to past, present, and future environmental conditions and implications for
637 atmospheric chemistry, J. Geophys. Res., 117, D22302, 2012.
638
639 Palmer, J. R., and Totterdell, I. J.: Production and export in a Global Ocean Ecosystem Model,
640 Deep Sea Res., Part I, 48, 1169–1198, 2001.
641
642 Price, C., and Rind, D.: A simple lightning parameterization for calculating global lightning
643 distributions, J. Geophys. Res., 97, 9919-9933, 1992.
644
645 Price, C., and Rind, D.: Modeling global lightning distributions in a general circulation model,
646 Mon. Weather Rev., 122, 1994.
647
648 Riahi, K., Gruebler, A. and Nakicenovic, N.: Scenarios of long-term socio-economic and
649 environmental development under climate stabilization, Technol. Forecast. Soc. Change, 74(7),
650 887–935, 2007.
651
652 Rich, S.: Ozone damage to plants, Ann. Rev. Phytopathol., 2, 253-266, 1964.
653
654 Rizzo, L. V., Artaxo, P., Muller, T., Wiedensohler, A., Paixao, M., Cirino, G. G., Arana, A.,
655 Swietlicki, E., Roldin, P., Fors, E. O., Wiedemann, K. T., Leal, L. S. M. and Kulmala, M.: Long
656 term measurements of aerosol optical properties at a primary forest site in Amazonia, Atmos.
657 Chem. Phys., 13, 2391–2413, 2013.
658
659 Rummel, U., Ammann, C., Kirkman, G. A., Moura, M. A. L., Foken, T., Andreae, M. O., and
660 Meixner, F. X.: Seasonal variation of ozone deposition to a tropical rain forest in southwest
661 Amazonia, Atmos. Chem. Phys., 7, 5415–5435, 2007.
662
663 Seinfeld, J. H., Pandis, S. N.,: Atmospheric Chemistry and Physics: from Air Pollution to Climate
664 Change. J. Wiley, New York, 1998.
665
666 Sierra, C. A., Harmon, M. E., Moreno, F. H., Orrego, S. A., Del Valle, J. I.: Spatial and temporal
667 variability of net ecosystem production in a tropical forest: testing the hypothesis of a significant
668 carbon sink. Glob. Change Biol., 13, 838–853, 2007.

669
670 Sigler, J. M., Fuentes, J. D., Heitz, R. C., Garstang, M., and Fisch, G.: Ozone dynamics and
671 deposition processes at a deforested site in the Amazon basin, Ambio, 31(1), 21-7, 2002.
672
673 Sitch, S., Cox, P. M., Collins, W. J., Huntingford, C.,: Indirect radiative forcing of climate change
674 through ozone effects on the land-carbon sink, Nature, 448, 791-95, 2007.
675
676 Taylor, J. A., Lloyd, J.: Sources and sinks of atmospheric CO_2. Australian Journal of Botany, 40, 4-
677 5, 407-418, 1992.
678
679 Taylor, K. E., Stouffer, R., J. and Meehl, G. A.: An Overview of CMIP5 and the Experiment
680 Design, B. Am. Meteorol. Soc., 93.4, 2012.
681
682 Thompson, T. M., and Selin. N. E.: Influence of air quality model resolution on uncertainty
683 associated with health impacts, Atmos. Chem. Phys., 12, 9753-9762, 2012.
684
685 Tie, X., Brasseur, G. and Ying, Z.: Impact of model resolution on chemical ozone formation in
686 Mexico City: application of the WRF-Chem model, Atmos. Chem. Phys., 10, 8983-8995, 2010.
687
688 van der Werf, G. R., Randerson, J. T., Giglio, L., Collatz, G. J., Kasibhatla, P. S., and Arellano, A.
689 F.: Interannual variability in global biomass burning emissions from 1997 to 2004, Atmos. Chem.
690 Phys., 6, 3423–3441, 2006.
691
692 van der Werf et al.: Global fire emissions and the contribution of deforestation, savanna,
693 forest, agricultural, and peat fires (1997–2009), Atmos. Chem. Phys., 10, 11707–11735, 2010.
694
695 Valari, M., and Menut, L.: Does an increase in air quality Models' resolution bring surface ozone
696 concentrations closer to reality?, J. Atm. Oceanic Tech., 25, 2008.
697
698 Wesely, M. L.: Parameterization of surface resistances to gaseous dry deposition in regional-scale
699 numerical models, Atmos. Environ., 23, 1293–1304, 1989.
700
701 Yienger, J. J., and Levy II, H.: Global inventory of soil-biogenic NOx emissions, J. Geophys. Res.,
702 100, 11,447–11,464, 1995.
703

Figures

1. Comparison of measured (dots) and simulated (stars) monthly averaged diurnal cycle of surface O_3 mixing ratios at the Porto Velho site, including measured day-to-day variability (grey lines) and standard deviation (dashed lines) for the model results. The measurements have an uncertainty of 4%.

2. Comparison of measured (dots) and simulated (stars) monthly averaged diurnal cycle of surface O_3 mixing ratios at the ZF2 site in the Cuieiras forest reserve, including measured day-to-day variability (grey lines) and standard deviation (dashed lines) for the model results. The measurements have an uncertainty of 4%. We show one of the two available years of observations. Legend as in Figure 1.

3. Vegetation cover in HadGEM2 for the month of September. The red rectangle is our region of analysis. The two sites used in the model evaluation (the sites of Porto Velho and ZF2 site in the Cuieiras forest reserve) are also marked.

4. Monthly average surface O_3 mixing ratio simulated with HadGEM2 for the month of September (average over 8 years of simulations).

5. Clockwise from the top-left: (a) Simulated monthly surface O_3 mixing ratios; (b) Simulated monthly total NPP; (c) Simulated monthly variation in total NPP. The plots show the results for the control simulation (i.e. using the decadal mean biomass burning emissions from Lamarque et al. (2010) centered on year 2000; 2000 BB emissions) and the various experiments with increased (+) or decreased (-) biomass burning emissions over South America by 20, 40, 60, 80 and 100%. All data are averaged over the region of analysis for 8 years of simulations.

6. From the left: simulated variation in surface O_3 mixing ratios and NPP over the region of analysis for the months of August, September and October.

7. Probability density function (histogram) of the variation in NPP for the same months. The plots show the variation between the experiments with South American biomass burning increased/decreased by 40, 60 and 100% and the control simulation.

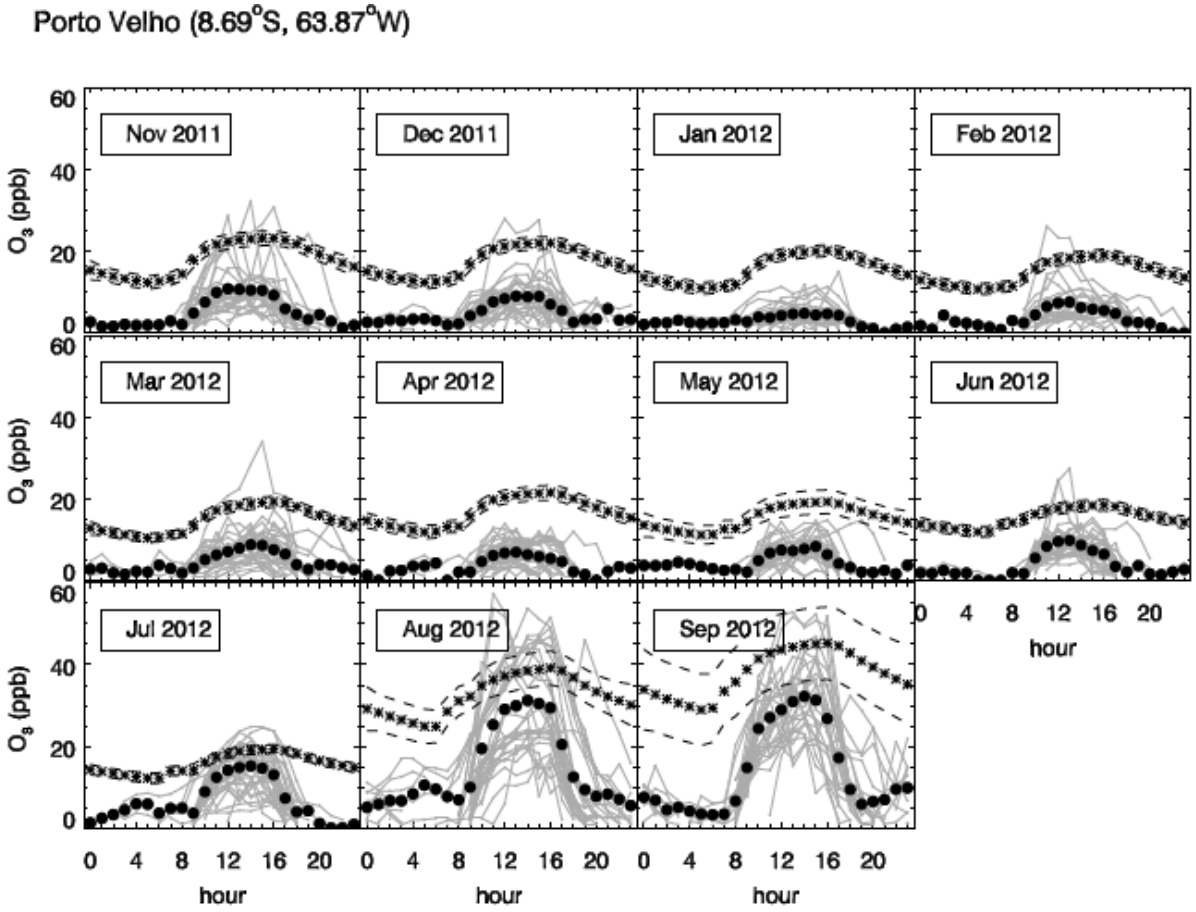

736
737 Figure 1
738

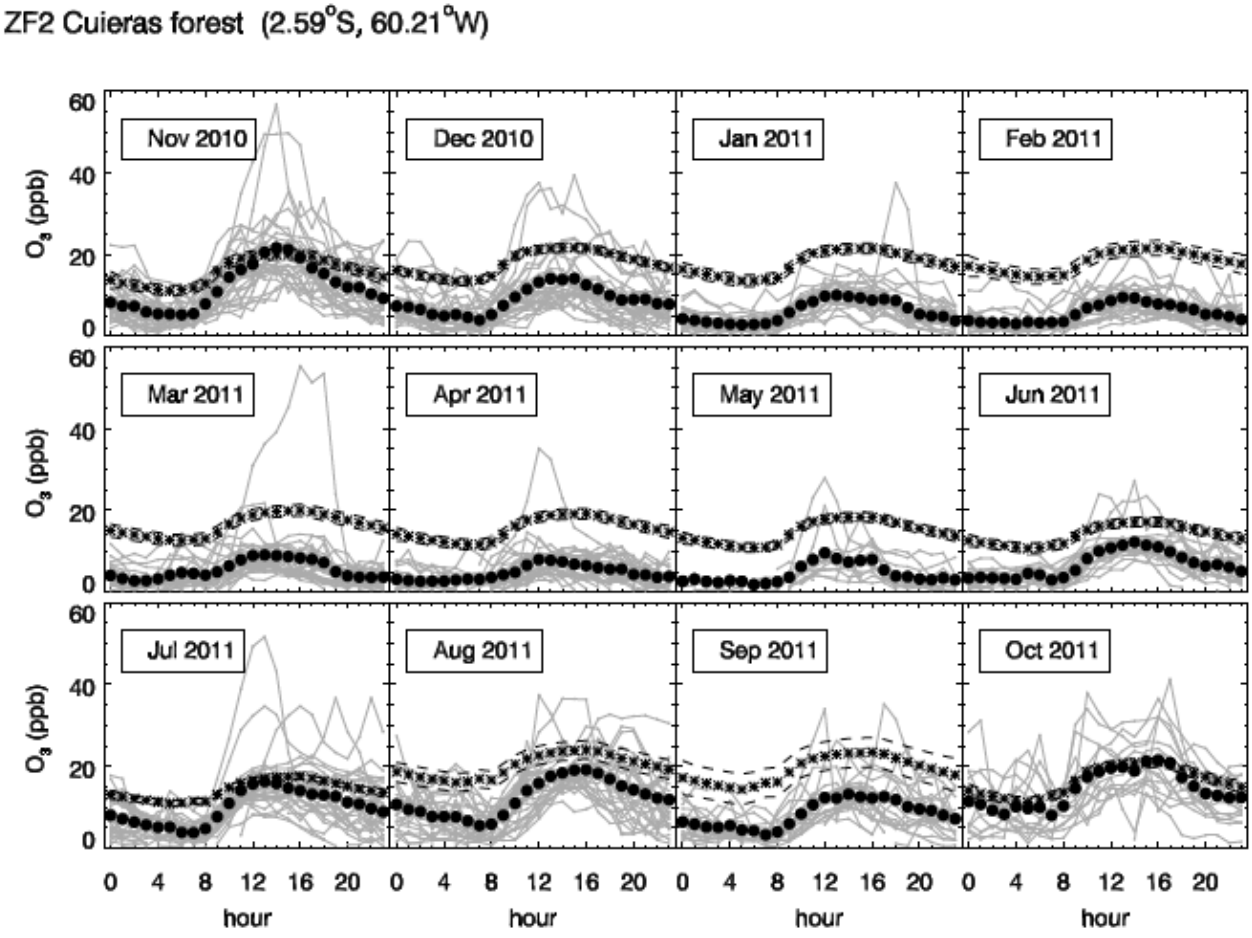
ZF2 Cuieras forest (2.59°S, 60.21°W)
Nov 2010
Dec 2010
Jan 2011
Feb 2011
Mar 2011
Apr 2011
May 2011
Jun 2011
Jul 2011
Aug 2011
Sep 2011
Oct 2011
O3 (ppb)
hour
0
20
40
60
0 4 8 12 16 20

Figure 2

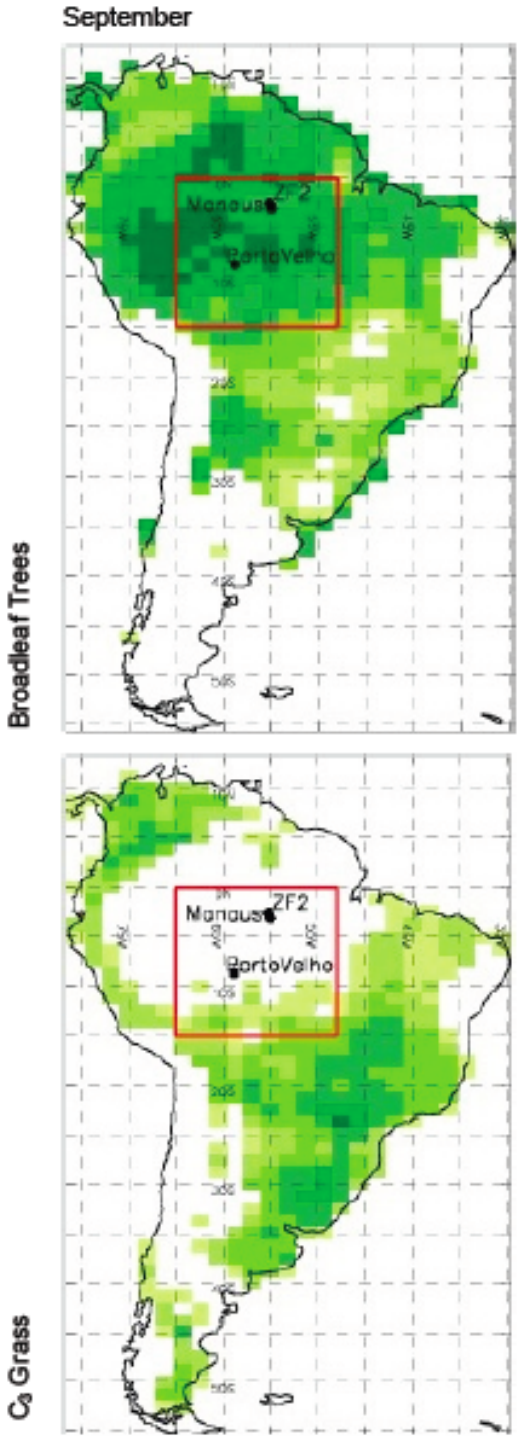
September
Broadleaf Trees
Manaus
ZF2
PortoVelho
C4 Grass
Manaus
ZF2
PortoVelho

Figure 3

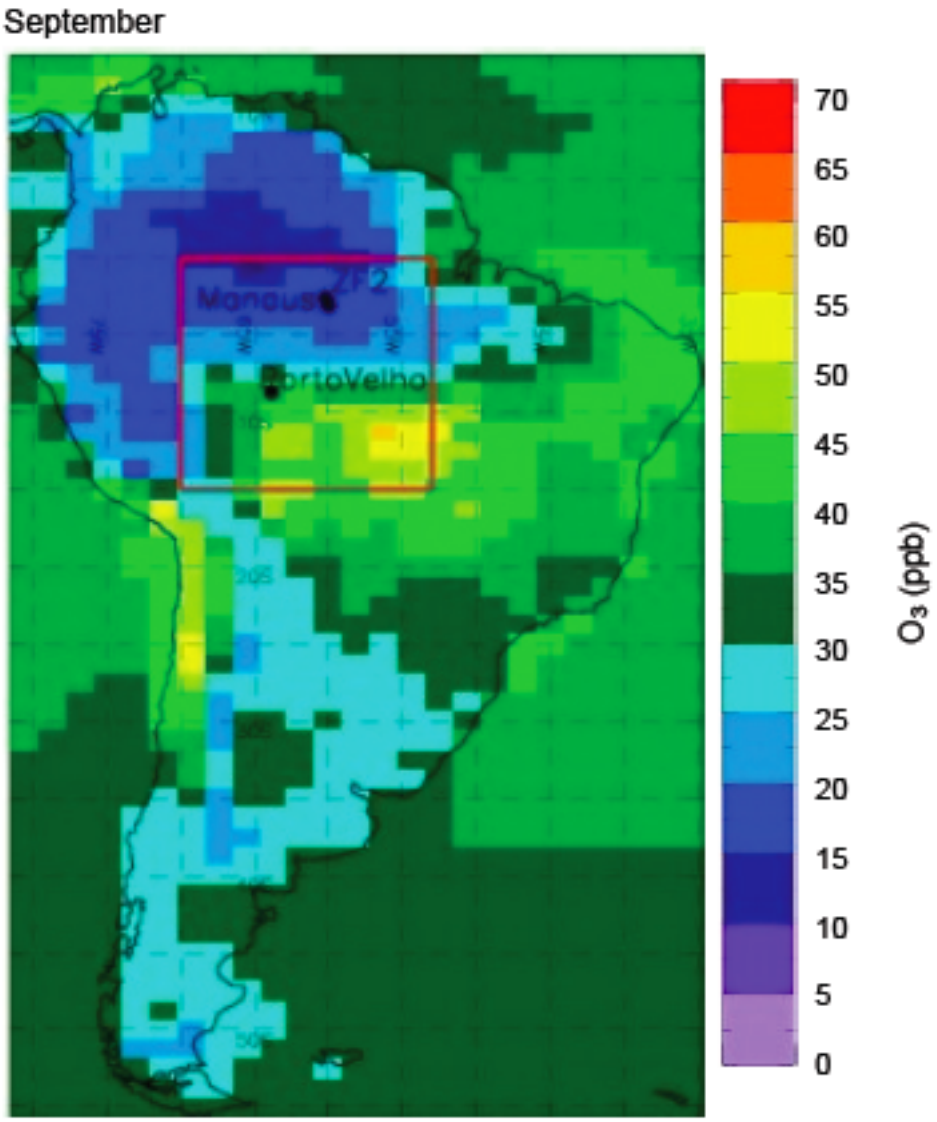
September
Manaus
PortoVelho
70
65
60
55
50
45
40
35
30
25
20
15
10
5
0
O3 (ppb)

Figure 4

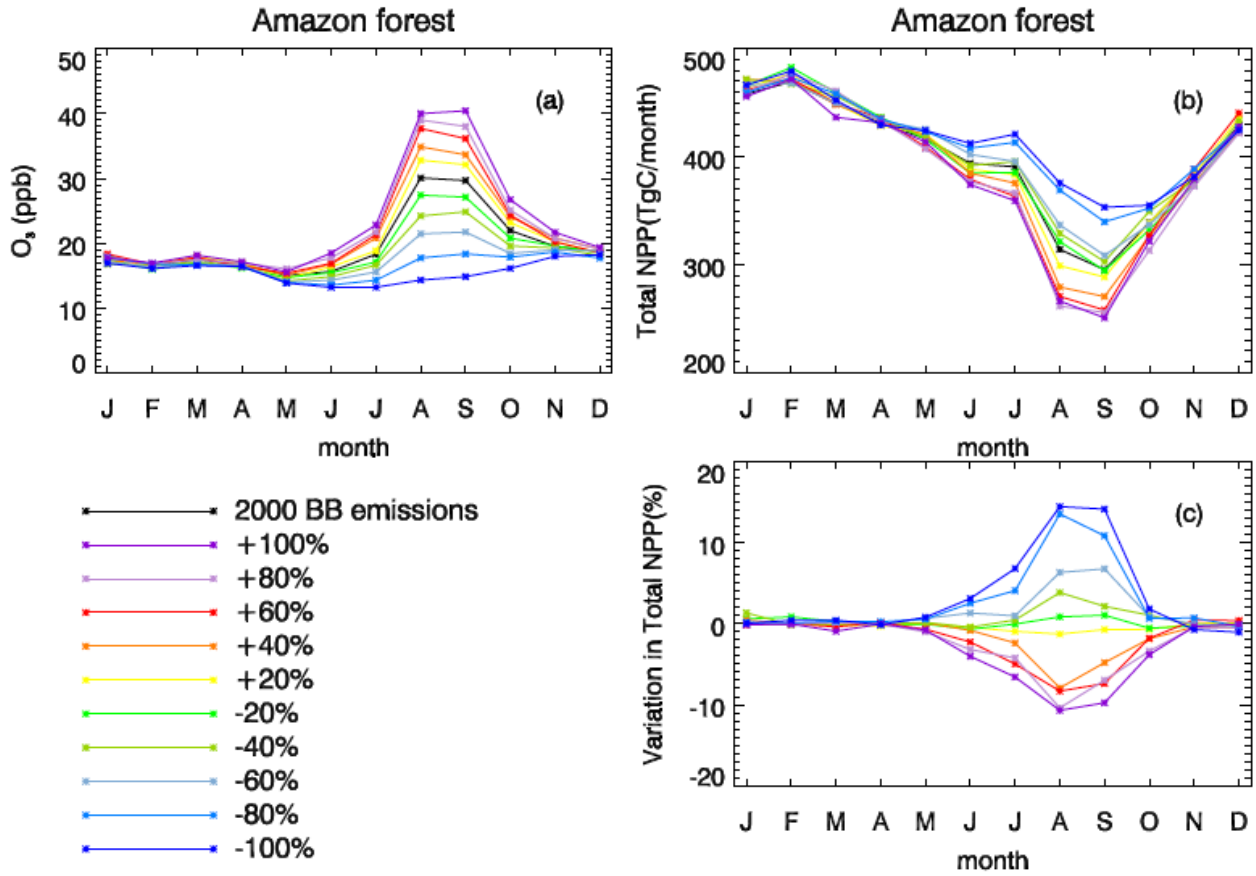
Amazon forest
(a)
O_3 (ppb)
month
2000 BB emissions
+100%
+80%
+60%
+40%
+20%
-20%
-40%
-60%
-80%
-100%
Amazon forest
(b)
Total NPP(TgC/month)
month
(c)
Variation in Total NPP(%)
month

Figure 5

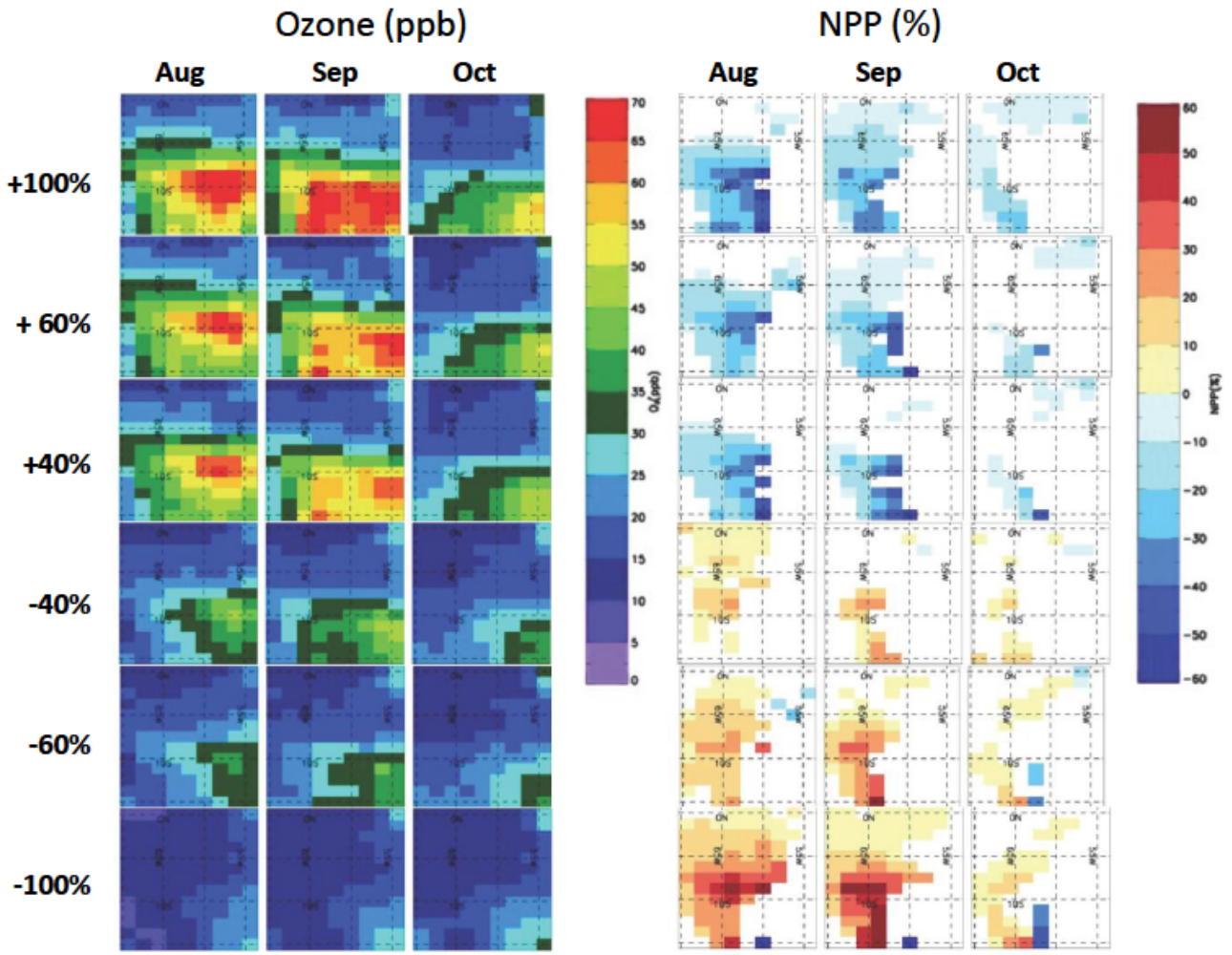

Figure 6

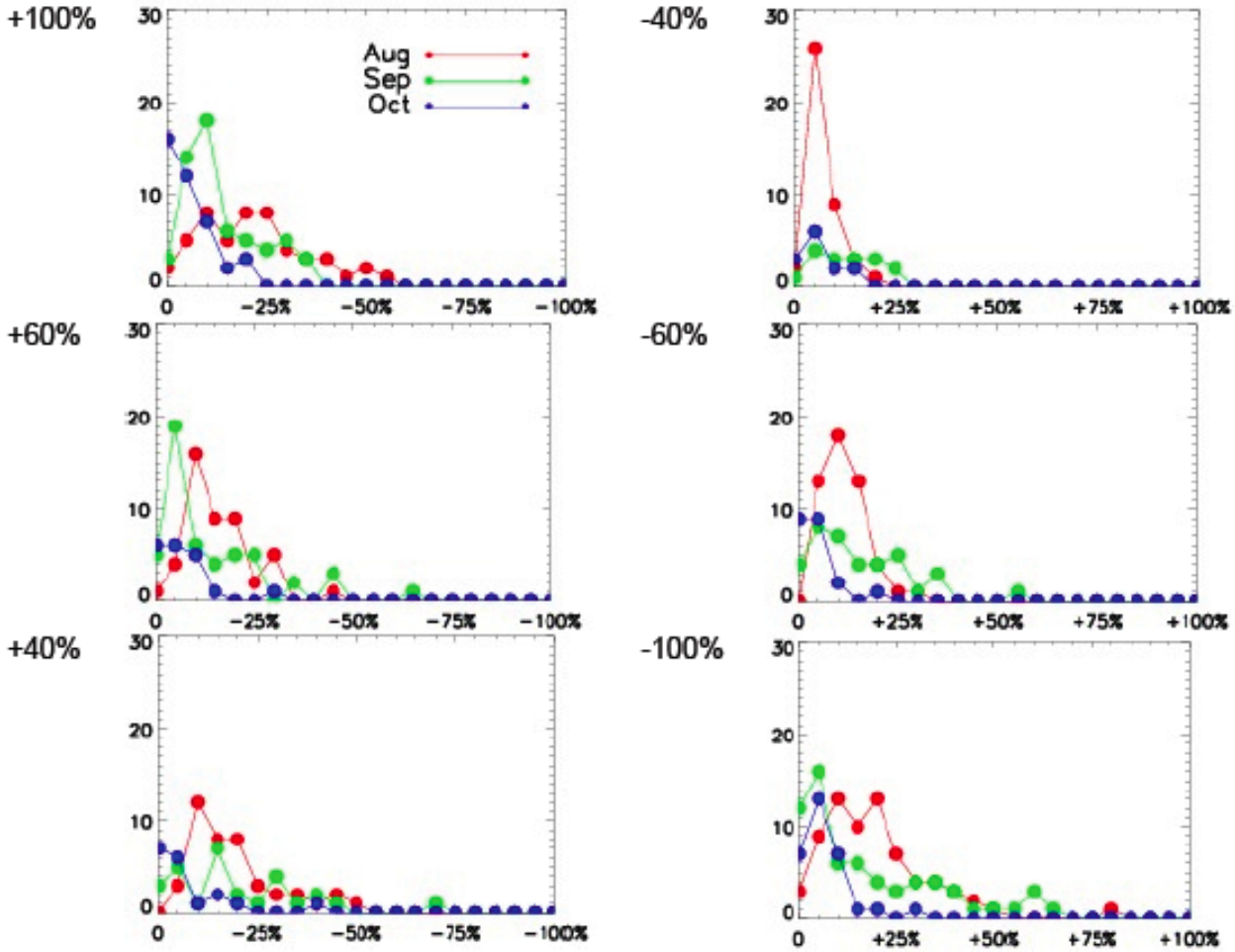

748
749 Figure 7